Impact of Mitochondrial Ca^{2+} Cycling on Pattern Formation and Stability

M. Falcke,* J. L. Hudson,# P. Camacho,§ and J. D. Lechleiter¶

*Max Planck Institute for Physics of Complex Systems, 01187 Dresden, Germany; #Department of Chemical Engineering, University of Virginia, Charlottesville, Virginia 22903-2442 USA; §Department of Physiology, University of Texas Health Sciences Center at San Antonio, San Antonio, Texas 78284-7756 USA; and ¶Department of Molecular Medicine, Institute of Biotechnology, University of Texas Health Sciences Center at San Antonio, San Antonio, Texas 78245-3207 USA

ABSTRACT   Energization of mitochondria significantly alters the pattern of Ca^{2+} wave activity mediated by activation of the inositol (1,4,5) trisphosphate (IP$_3$) receptor (IP$_3$R) in *Xenopus* oocytes. The number of pulsatile foci is reduced and spiral Ca^{2+} waves are no longer observed. Rather, target patterns of Ca^{2+} release predominate, and when fragmented, fail to form spirals. Ca^{2+} wave velocity, amplitude, decay time, and periodicity are also increased. We have simulated these experimental findings by supplementing an existing mathematical model with a differential equation for mitochondrial Ca^{2+} uptake and release. Our calculations show that mitochondrial Ca^{2+} efflux plays a critical role in pattern formation by prolonging the recovery time of IP$_3$Rs from a refractory state. We also show that under conditions of high energization of mitochondria, the Ca^{2+} dynamics can become bistable with a second stable stationary state of high resting Ca^{2+} concentration.

INTRODUCTION

Cytoplasmic Ca^{2+} is a ubiquitous second messenger that regulates multiple cellular processes (Tsien and Tsien, 1990; Berridge, 1993; Fewtrell, 1993; Putney and Bird, 1993; Pozzan et al., 1994; Clapham, 1995). In many cells, hormone-stimulated IP$_3$ production generates waves of intracellular Ca^{2+} release, which propagate across the cell (Cornell-Bell et al., 1990; Kasai and Augustine, 1990; Lechleiter et al., 1991; Blatter and Wier, 1992; DeLisle and Welsch, 1992; Amundson and Clapham, 1993; Eidne et al., 1994; Yao and Parker, 1994; Nathanson et al., 1995; Wang and Augustine, 1995; Thomas et al., 1996). Our initial observation of rotating spirals and expanding target patterns of Ca^{2+} waves in *Xenopus laevis* oocytes demonstrated that intracellular Ca^{2+} release behaves as an excitable medium (Lechleiter et al., 1991; Lechleiter and Clapham, 1992; Camacho and Lechleiter, 1995). Excitable media are locally stable such that a small perturbation results in the direct return of the system to the steady state. However, a suprathreshold disturbance causes the system to sojourn through a large nonlinear excursion before it returns to the stable steady state (Mikhailov, 1994). Target and/or spiral patterns of intercellular Ca^{2+} release have also recently been reported in rat liver tissue, in epithelial cells, and in hippocampal slice cultures (Sanderson et al., 1994; Robb-Gaspers and Thomas, 1995; Thomas et al., 1995; Harris-White et al., 1998), suggesting that the concept of an excitable medium is applicable to Ca^{2+} signaling in multicellular systems. Spatiotemporal Ca^{2+} signals have also been recently shown to control gene expression differen-

tially (Gu and Spitzer, 1995; Dolmetsch et al., 1998; Li et al., 1998). Other biologically excitable systems exhibiting complex spatiotemporal patterns include the spread of excitation in heart muscle, the release of extracellular cAMP during *Dictyostelium discoideum* aggregation, and the K$^+$ ion fluxes in retinal cells (Loomis, 1979; Devreotes et al., 1983; Goroleva and Bures, 1983; Davidenko et al., 1992; Rensing, 1993; Winfree, 1993; Karma, 1994; Newman and Zahs, 1997). Thus, a fundamental understanding of the mechanisms governing pattern selection as well as the creation and stability of spiral waves has been a topic of major interest in recent years (Rensing, 1993; Winfree, 1993; Karma, 1994), given their impact on such a wide variety of biological phenomena.

We have previously reported that changes in intracellular Ca^{2+} signaling are dependent on the rate of mitochondrial Ca^{2+} uptake (Jouaville et al., 1995). Increasing the rate of Ca^{2+} uptake by injection of respiratory chain substrates increases Ca^{2+} wave amplitude and velocity. Curiously, increased cytosolic Ca^{2+} sequestration increases the excitation threshold and once excited, mitochondrial Ca^{2+} uptake would be expected to decrease the peak amplitude and slow the wave velocity. In this paper we theoretically account for these seemingly paradoxical observations by incorporating the complete dynamics of mitochondrial Ca^{2+} cycling into the Tang and Othmer (TO) model of Ca^{2+} wave activity (Tang et al., 1996). Our simulations show that mitochondrial Ca^{2+} efflux is a significant determinant of pattern formation and that the cytosol can exhibit a bistable behavior.

MATERIALS AND METHODS

Experimental

Xenopus oocyte preparation and confocal imaging of intracellular Ca^{2+} was as previously described (Jouaville et al., 1995). Briefly, oocytes were injected with Calcium Green II (50 nl, ~12.5 μM final concentration,

assuming a 1:20 dilution; Molecular Probes, Eugene, OR) 30–60 min before each experiment. Images were acquired with a NORAN OZ confocal laser scanning microscope at zoom 0.7 attached to a Nikon Eclipse 200 with a 20× (0.75 NA) Nikon objective lens at 1-s intervals. The confocal aperture was set at 15 μm. Images were analyzed with ANALYZE software (Mayo Foundation, Rochester, MN) on a Silicon Graphics workstation. Ca^{2+} increases are reported as $\Delta F/F$, which represents $(F_{peak} - F_{rest})/F_{rest}$. Ca^{2+} wave activity was induced by injecting a 50-nl bolus of IP_3 (Calbiochem, San Diego, CA) of 6 μM (~300 nM final). All recordings were made in the absence of extracellular Ca^{2+}: 96 mM NaCl, 2 mM KCl, 2 mM $MgCl_2$, 5 mM Hepes (pH 7.5) (GibcoBRL, Grand Island, NY), 1 mM EGTA (Sigma, St. Louis, MO).

Numerical

We used a scaled version of the mathematical model for numerical calculations. Integrations were performed using a Euler forward scheme, with a spatial discretization of 0.125 and a time step of 0.0005. Onset of wave propagation was in general for a spatial discretization of 0.8. Stationary states were determined as the concentration values yielding the right-hand sides of the equations in the Appendix set equal to 0. Their stability was determined by the eigenvalues of the Jacobian matrix.

RESULTS AND DISCUSSION

Most current models of Ca^{2+} signaling (Dupont et al., 1991; DeYoung and Keizer, 1992; Atri et al., 1993; Li and Rinzel, 1994; Tang et al., 1996) are based on the observation that at low Ca^{2+} concentrations, IP_3 and Ca^{2+} work as co-agonists leading to Ca^{2+}-induced Ca^{2+} release (CICR), while at high concentrations, Ca^{2+} inhibits further Ca^{2+} release and the IP_3R becomes refractory (Iino, 1990; Parker and Ivorra, 1990; Bezprozvanny et al., 1991; Finch et al., 1991). The TO model is also based on this dual modulatory role of Ca^{2+} on IP_3-mediated Ca^{2+} release (Tang and Stephenson, 1996). We extended the TO model of Ca^{2+} signaling to incorporate the mechanisms of mitochondrial Ca^{2+} cycling by adding a third equation governing the uptake and release of Ca^{2+} by mitochondria and a corresponding term in the differential equation for cytosolic Ca^{2+} (see Appendix). The third equation was empirically formulated, essentially based on the experimental data reviewed by Gunter and Pfeiffer (1990). The reader is referred to a series of papers published by Magnus and Keizer for a detailed biophysical model of mitochondrial Ca^{2+} handling (Magnus and Keizer, 1997, 1998a, b). An important feature of mitochondrial Ca^{2+} cycling is that Ca^{2+} uptake and efflux are distinct pathways, the latter being 10–100 times kinetically slower (Gunter and Pfeiffer, 1990). The Ca^{2+} uptake mechanism is believed to be a uniporter that facilitates the diffusion of Ca^{2+} down the electrochemical gradient across the mitochondrial membrane (Gunter and Pfeiffer, 1990). Its dependence on cytosolic Ca^{2+} is modeled as a Hill function with the higher-order kinetics associated with cooperativity and saturation (Bygrave et al., 1971; Scarpa and Graziotti, 1973). A Hill coefficient of 2 is used based on a review of experimental data (Gunter and Pfeiffer, 1990). The value for the maximum uptake velocity ($V_{max}^{(1)}$) were chosen according to Marinos and Billett (1981), Marinos (1985), and Gunter and Pfeiffer (1990). We assume that the relevant Ca^{2+}

efflux mechanism for mitochondria in *Xenopus* oocytes is the Na^+/Ca^{2+} exchanger. This process was also modeled as a Hill function using a second-order Na^+ dependence (Gunter and Pfeiffer, 1990). Consequently, the exchanger is electroneutral and the Ca^{2+} efflux does not depend on the mitochondrial membrane potential. A wide range of values, from 1 to 189 μM, have been reported for the half-maximum value (K_d) (Gunter and Pfeiffer, 1990). However, physiological (Rizzuto et al., 1992, 1993; Jouaville et al., 1995) and morphological evidence (Satoh et al., 1990) indicates that mitochondria are located in close proximity to the ER, where they experience Ca^{2+} concentrations considerably higher than those in bulk cytoplasm. Rizzuto et al. (1992, 1993) estimated that the uptake velocity of Ca^{2+} released from internal stores was an order of magnitude higher than that resulting from the average bulk concentration of Ca^{2+}. We incorporated locally high Ca^{2+} concentrations into the model by multiplying the value of the Ca^{2+} concentration in the mitochondrial uptake term by a factor of 2.5, based on the data published by Rizzuto et al. (1993). This correction is equivalent to rescaling the half-maximum value of K_d to $K_d/2.5$. The resulting small value of K_d was essential for obtaining the results presented below.

In the experiments we modeled, mitochondria were energized by injection of oxidizable substrates increasing the membrane potential by ~30 mV (Jouaville et al., 1995). This corresponds to an increase of $V_{max}^{(1)}$ by about a factor of 5. We present results for different values of $V_{max}^{(1)}$ to parallel these experiments with and without energization of the mitochondria. Fig. 1 *A* shows the effect of mitochondria Ca^{2+} cycling on pulse profiles. For high mitochondrial Ca^{2+} uptake, the simulated pulse shows two phases of Ca^{2+} decay (Fig. 1 *A*), which were also observed experimentally (Jouaville et al., 1995). First, a rapid decay phase of cytosolic Ca^{2+} caused by Ca^{2+} uptake into the ER and mitochondria occurs (Camacho and Lechleiter, 1993; Hehl et al., 1996; Herrington et al., 1996). The second, slower phase of cytosolic Ca^{2+} decay can be attributed to mitochondrial Ca^{2+} efflux. The net flux of Ca^{2+} into mitochondria is initially inward, since Ca^{2+} efflux is much slower than uptake. However, as IP_3-mediated Ca^{2+} release decreases, the net movement of Ca^{2+} changes to mitochondrial efflux. This results in a prolonged elevation of cytosolic Ca^{2+} and delays the recovery of the IP_3R from the refractory state. For comparison, the dashed line in Fig. 1 *A* shows the Ca^{2+} pulse profile without energization of the mitochondria. These simulations suggest that mitochondrial Ca^{2+} cycling may modulate Ca^{2+} signaling by prolonging the recovery time of the IP_3 receptor.

Two fundamental characteristics of an excitable medium are the dependence of the wave velocity (v) on the curvature of the wavefront and on the frequency (f) of periodic wave trains (Dockery et al., 1988). The latter is called the dispersion relation $v(f)$. Simulations of repetitive Ca^{2+} waves at various levels of stimulation exhibited the expected dependence of wave velocity on frequency (Fig. 1 *B*) observed in many other excitable systems (Mikhailov, 1994). As the
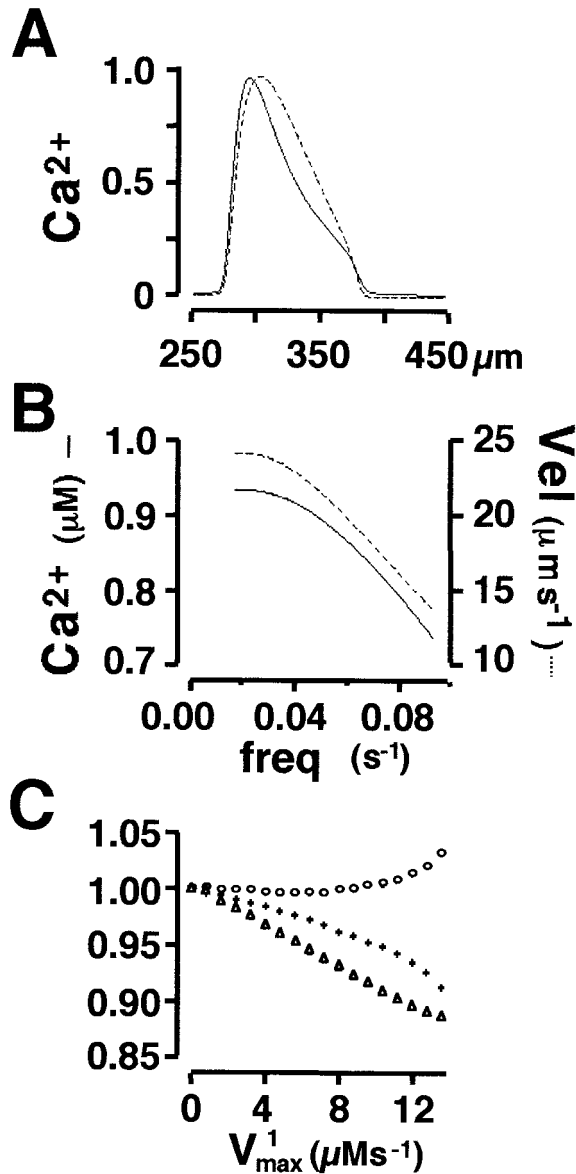
FIGURE 1 (*A*) Comparison of simulated of Ca^{2+} pulse profiles between modified and unmodified TO model (Tang et al., 1996). The pulses travel from right to left. The solid line represents a simulation taking into account mitochondrial Ca^{2+} cycling ($V_{max}^{(1)} = 28 \ \mu M \ s^{-1}$) and the dashed line represents a simulation without mitochondrial Ca^{2+} cycling ($V_{max}^{(1)} = 0 \ \mu M \ s^{-1}$). The amplitude of both pulses was normalized using their respective maximum. (*B*) Dependence of velocity (*dashed line*) and amplitude (*solid line*) of periodic Ca^{2+} pulses on frequency calculated with $V_{max}^{(1)} = 8.0 \ \mu M \ s^{-1}$. (*C*) Dependence of Ca^{2+} spiral wave velocity (*circles*), frequency (*crosses*), and amplitude (*triangles*) on $V_{max}^{(1)}$ for low Ca^{2+} mitochondrial uptake ($V_{max}^{(1)} < V_{max,cr}^{(1)}$) normalized to the value $V_{max}^{(1)} = 0 \ \mu M \ s^{-1}$.

frequency of the Ca^{2+} waves increases, both the velocity and amplitude decrease.

In *Xenopus* oocytes, stable spirals are observed under conditions of low mitochondrial Ca^{2+} uptake (Lechleiter et al., 1991; Lechleiter and Clapham, 1992; Camacho and Lechleiter, 1995). Our model simulations also indicate that spiral patterns are stable under these conditions. The formation of spiral wave patterns is due to the curvature-
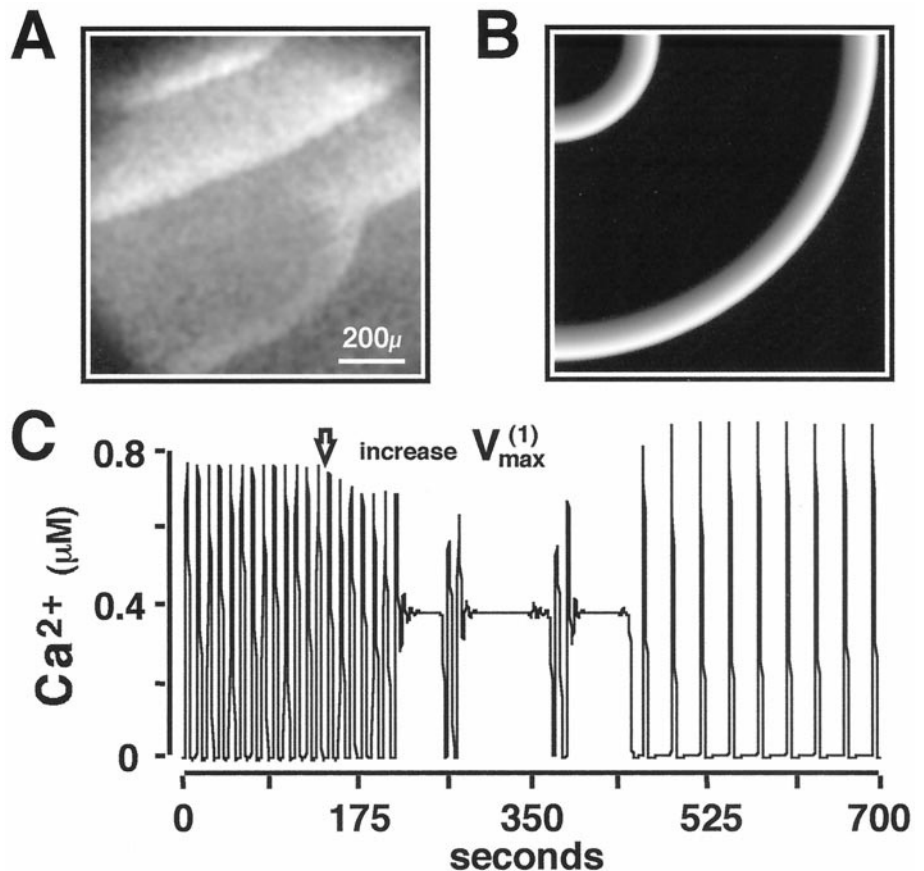
velocity relationship (Dockery et al., 1988); spirals originate at the free end of propagating waves, where the wavefront curvature is largest, resulting in lower velocity and the formation of the trademark curling pattern. With increasing $V_{max}^{(1)}$, a decrease in rotational frequency is accompanied by a small increase in wave velocity and a small decrease in wave amplitude (Fig. 1 *C*); this behavior only holds for small values of $V_{max}^{(1)}$, below a critical value to be described in the following paragraph.

When mitochondria are energized in *Xenopus* oocytes, spiral wave patterns become unstable, disappear, and do not reform. This model predicts, in agreement with these experiments, that spirals cease to exist at a certain critical value of mitochondrial Ca^{2+} uptake ($V_{max,cr}^{(1)} = 14 \ \mu M \ s^{-1}$). Above this value, it is found that waves emitted from pacemakers form the pattern. Examples of these waves, as observed in experiments and simulation, are shown in Fig. 2, *A* and *B*, and at the website http://www.mpipks-dresden.mpg.de/~falcke/thesite.html. A simulation was also carried out corresponding to an experiment (Jouaville et al., 1995) in which pyruvate/malate was injected into an oocyte. In this simulation, $V_{max}^{(1)}$ was increased. The changing Ca^{2+} concentration at a point is shown in Fig. 2 *C*. In two-dimensional simulations, the Ca^{2+} oscillations associated with spiral waves cease as the system moves to a new steady state. This is followed by the dominance of waves emitted from a pacemaker.

Fig. 3 *A* shows the transient state of a spiral wave tip when Ca^{2+} uptake exceeds the critical value ($V_{max}^{(1)} > V_{max,cr}^{(1)}$). When the tip bends in the early stage of spiral formation, another small amplitude wave emerges from the back of the wave at the highest curvature (indicated by white arrow). Mitochondrial Ca^{2+} efflux is responsible for this secondary wave, which in turn is responsible for prolonging the refractory state of the IP_3R and preventing spiral formation. Although efflux plays a fundamental role in the destabilization of the spiral core, it is not the sole determinant. Planar waves exist at frequencies higher than those at which spiral waves occur. This indicates that wavefront curvature also contributes to spiral core instability. Near the spiral tip, where the wavefront curvature is the highest, Ca^{2+} efflux is focused. This focal increase in Ca^{2+} further prolongs the refractory period of IP_3Rs. Thus, both curvature and mitochondrial efflux are responsible for the generation of the secondary wave which forces the tip outward, thereby preventing spiral pattern formation (Fig. 3 *B*). This phenomenon was experimentally observed in the oocyte after energization as shown in Fig. 3, *C* and *D*. The free end of a Ca^{2+} wave is forced outward by a secondary Ca^{2+} wave and the spiral fails to form.

When periodic wave patterns of different frequencies are present in a medium, they compete for space. As time goes on, the pattern with the highest frequency generally gains spatial control of the field (Mikhailov, 1994). We recently showed that spiral waves dominate pacemakers in *Xenopus* oocytes (Lechleiter, 1998); this indicates that the former have higher frequencies. Thus, it is only after the spirals

FIGURE 2 Comparison of two-dimensional simulated Ca^{2+} waves with empirically obtained data in *Xenopus* oocytes. (*A*) Image of Ca^{2+} wave activity initiated by IP_3 in an oocyte in which mitochondria are energized by injection of pyruvate/malate (10 mM final concentration). Experimental conditions and protocols were as previously described (Jouaville et al., 1995). (*B*) Simulation of Ca^{2+} pacemaker activity from a focus located in the upper left corner of the figure. This simulation takes into account high mitochondrial Ca^{2+} uptake conditions ($V_{max}^{(1)} = 8.0$ μM s^{-1}) for an area of 700×700 μm^2. (*C*) Local time series of Ca^{2+} concentration for the simulation shown in (*B*). At the time indicated by the arrow ($t = 150$ s), mitochondrial Ca^{2+} uptake was increased ($V_{max}^{(1)} = 16.0$ μM s^{-1}) to model an experimental injection of pyruvate/malate (Jouaville et al., 1995). After a transient, the spirals disappeared and the pacemaker activity dominated pattern formation. In this high mitochondrial activity mode, increases in amplitude and period are observed. The velocity of wave propagation also increases from 14 μm s^{-1} to 23 μm s^{-1}. See also http://www.mpipks-dresden.mpg.de/~falcke/thesite.html for the complete simulation.
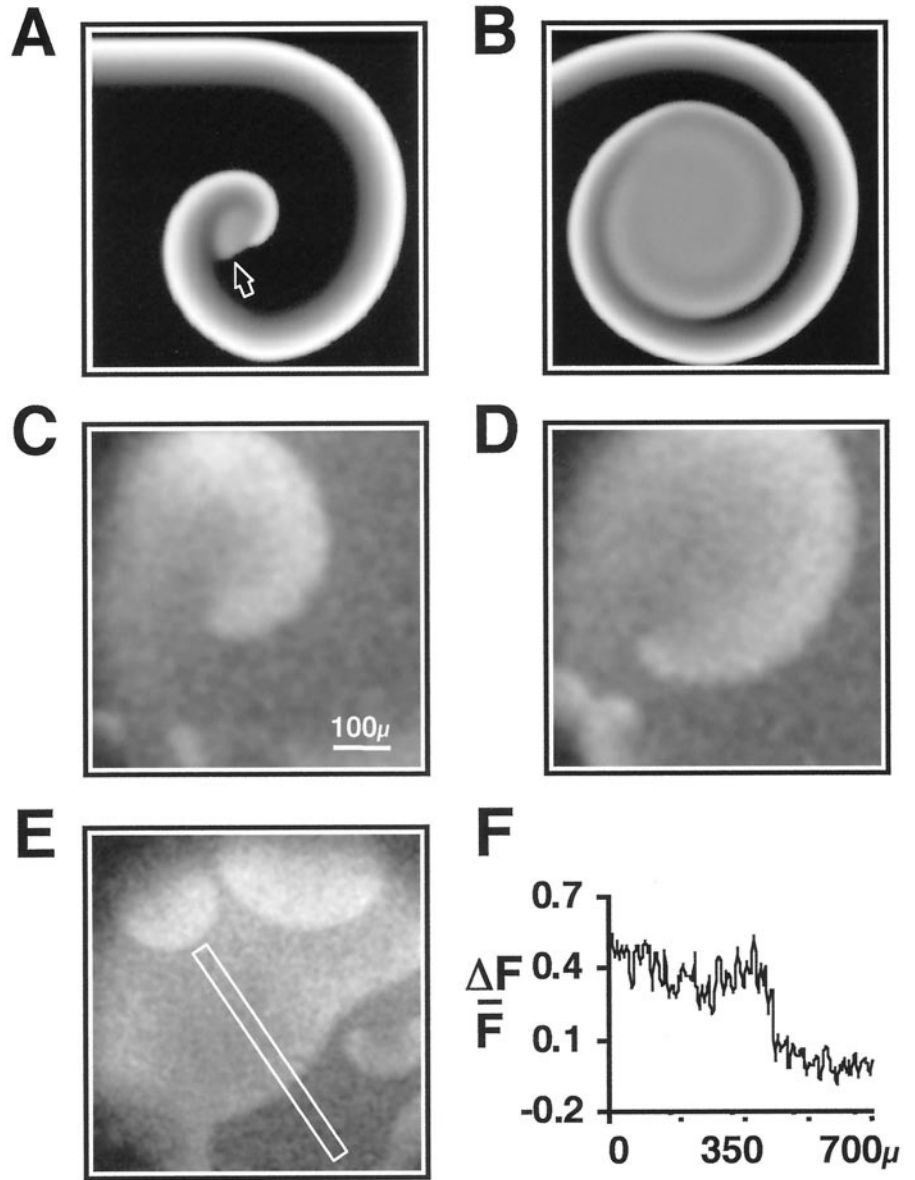
disappeared above $V_{max,cr}^{(1)}$—when mitochondria are energized—that the lower-frequency pacemakers can govern the pattern formation in the oocyte. The dependence of the amplitude, frequency, and velocity of waves in oocytes on the state of energization of mitochondria can now be readily explained. Energization results in a wave pattern dominated by slow pacemakers. The smaller frequency leads to an increase in wave amplitude and velocity, according to the dispersion relation.

The local dynamics of our model yield three stationary states, each with different concentrations of cytosolic Ca^{2+}. At low mitochondrial Ca^{2+} uptake (small $V_{max}^{(1)}$), only the state with the lowest cytosolic Ca^{2+} is stable and the cytosol behaves as an excitable system. Our calculations indicate that the system becomes bistable at the uptake value $V_{max,b}^{(1)} = 9.6$ μM s^{-1} (i.e., $V_{max,b}^{(1)} < V_{max,cr}^{(1)}$). At this point, the stationary state with the highest cytosolic Ca^{2+} concentration is stabilized by increased mitochondrial Ca^{2+} cycling. The system now has two stable stationary states. When both states exist at adjacent locations, the interface moves so that the volume occupied by one of the states grows at the expense of the other (see Mikhailov, 1994 for bistable systems in general). This moving interface is called a front and the state, which loses volume, is termed metastable. Whether the system switches by a front from low to high cytosolic Ca^{2+}, or vice versa, depends on the degree of mitochondrial energization. In most of the bistable region

that we consider, the state of high cytosolic Ca^{2+} is metastable. In our bistable system, both waves (pulses) and fronts occur and below $V_{max,cr}^{(1)}$ spirals form. Above $V_{max,cr}^{(1)}$, the region of high Ca^{2+} can expand if it is surrounded by a wave, even though it is the metastable state. Thus, a front of transition from low to high Ca^{2+} can occur in this parameter range if it immediately follows a wave. This occurs when the unstable spiral core expands (Fig. 3, *A–D*). If the wave leading the front is extinguished by collision with another wave, the front reverses its direction of motion. Another way that this patch of high Ca^{2+} in Fig. 3 *B* disappears is that a pacemaker inside it starts a front that returns the region to a state of low Ca^{2+}. Finally, this creates a pattern in which the waves emitted by pacemakers become the dominant structure of the bistable system (http://www.mpipks-dresden.mpg.de/~falcke/thesite.html).

At very high energization of the mitochondria ($V_{max}^{(1)} > 16.4$ μM s^{-1}), the simulations show that fronts from low to high cytosolic Ca^{2+} continue to exist outside the spiral core. This indicates that the region of high cytosolic Ca^{2+} emerging from the spiral instability continues to expand even if the leading pulse becomes annihilated. Experimental evidence for such a transition in oocytes is shown in Fig. 3, *E* and *F*. Fronts from high to low Ca^{2+} cease to exist at $V_{max}^{(1)} = 23$ μM s^{-1}, i.e., for 16.4 μM s^{-1} < $V_{max}^{(1)} = 23$ μM s^{-1} fronts in both directions and waves co-exist. Which waveform arises depends on the situation initiating it. If a

FIGURE 3 Stability and formation of the spiral wave core. (A) Simulated development of the free end of a spiral at high mitochondrial Ca^{2+} uptake ($V_{max}^{(1)} = 20$ μM s^{-1}) for an area of 500×500 μm^2. When the curvature becomes too high, a secondary wave appears (white arrow) and prevents further development of the spiral by forcing the tip outward. (B) State of the spiral core 7 s after the simulation shown in (A). (C) Experimental image of an unstable spiral core in an oocyte. Ca^{2+} wave activity was initiated by simultaneous injection of IP$_3$ (6 μM final concentration) and pyruvate/malate (10 mM final). Notice that the free end of the Ca^{2+} wave fails to form a spiral pattern. (D) Image of the experimental Ca^{2+} wave shown in (C) collected 3 s later. Note that the tip of the free end was forced outward by the unstable core, as simulated in (B). (E) Bistability of Ca^{2+} wave activity in *Xenopus* oocytes with energized mitochondria. IP$_3$-induced Ca^{2+} wave activity observed in an oocyte preinjected with pyruvate/malate (10 mM final concentration). The direction of wave propagation is indicated by the white arrow. The fluorescence intensity ($\Delta F/F$) of the white frame is plotted in (F).
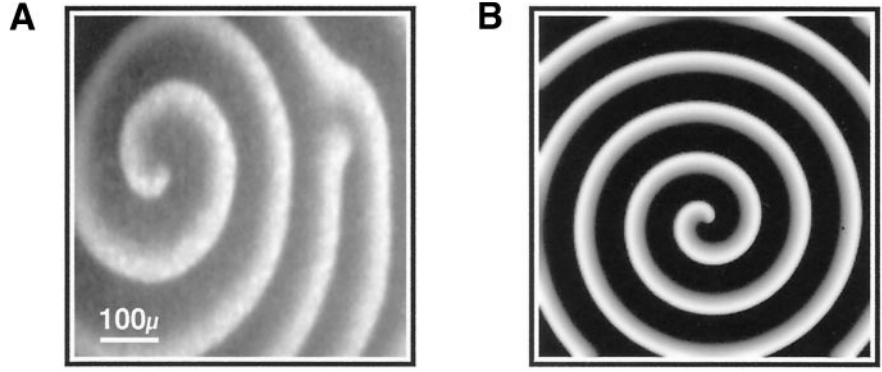
front is initiated at $V_{max}^{(1)} > 23$ μM s^{-1}, the resting Ca^{2+} concentration in the oocyte is predicted to switch to the stationary state with high cytosolic Ca^{2+}, and wave activity stops.

The mechanism of mitochondrial-induced spiral instability described above suggests that spirals could be recovered by increasing cytosolic Ca^{2+} removal. Experimental studies in *Xenopus* oocytes show that overexpression of Ca^{2+}-ATPases permits spiral wave formation even in the presence of energized mitochondria (Fig. 4 A). We simulated increased SERCA expression in our model by factoring an increase of 10% in the density of SERCAs. Calculations were performed assuming high mitochondrial Ca^{2+} uptake, where spiral wave formation is unstable. Consistent with our experimental observations, the simulation shows that an increase in SERCA density restores spiral formation (Fig. 4 B). This observation also supports the mechanism proposed

above, in which pattern instability is attributed to increased mitochondrial Ca^{2+} cycling.

In summary, we have resolved an experimental paradox on the effects of energization of mitochondria on Ca^{2+} wave activity in *Xenopus* oocytes. Namely, that increased mitochondrial Ca^{2+} sequestration leads to increased Ca^{2+} wave amplitude and velocity (Jouaville et al., 1995). This outcome is theoretically predicted when both mitochondrial Ca^{2+} uptake and Ca^{2+} efflux are incorporated into the TO model of Ca^{2+} activity. Our simulations also demonstrate that mitochondria play a critical role in pattern formation and stability. We find that increased mitochondrial Ca^{2+} efflux destabilizes the formation of spirals. Furthermore, energization of mitochondria creates a bistable cytosol in which resting Ca^{2+} concentrations can stably exist at levels higher than normal. Interestingly, the sperm-induced Ca^{2+} wave in *Xenopus* eggs has also recently been modeled as a

FIGURE 4 (*A*) Overexpression of SERCA 2b rescues IP$_3$-induced spiral pattern formation of Ca^{2+} waves in an oocyte preinjected with pyruvate/malate. (*B*) Simulation of a spiral Ca^{2+} wave at high mitochondrial Ca^{2+} uptake ($V_{max}^{(1)}$ = 20 μM s^{-1}) and increased SERCA density, which was simulated by factoring into the calculation a 10% higher maximum Ca^{2+} pump rate (P_{max}^r = 5.9 μM s^{-1}).

bistable system (Fontanilla and Nuccitelli, 1998; Wagner et al., 1998). Taken together, these model simulations provide a new understanding of the role played by mitochondrial Ca^{2+} cycling in pattern formation and in controlling intracellular Ca^{2+} levels.

APPENDIX

Mathematical model of Ca^{2+} signaling incorporating mitochondrial Ca^{2+} cycling

In the TO model (Tang and Othmer, 1994; Tang et al., 1996), Ca^{2+} efflux of the endoplasmic reticulum (ER) is described by the first term of the c-dynamics (Eq. A1). The dependence of Ca^{2+} release on both IP$_3$ and Ca^{2+} is modeled by assuming one site for IP$_3$ binding, one activating and one inhibitory site for Ca^{2+} binding. The channel is open when IP$_3$ and Ca^{2+} are bound at the activating site. Binding of Ca^{2+} at the inhibitory site closes the channel. It is assumed that IP$_3$ is spatially and temporally constant since experimental data show that the turnover rate of IP$_3$ in *Xenopus* oocytes is of the order of minutes (Allbritton et al., 1992). Extrusion of Ca^{2+} through the activity of plasma membrane ATPases and exchangers is modeled as a small leak term. The TO model assumes that the efflux of Ca^{2+} from the ER is proportional to the difference between lumenal and cytosolic Ca^{2+} concentration. This provides an additional feedback of the ER Ca^{2+} content on cytosolic Ca^{2+} dynamics. Once Ca^{2+} is released from the ER into the cytosol, the cycle of Ca^{2+} dynamics is closed by cytosolic Ca^{2+} removal. Resequestration of Ca^{2+} into internal stores is modeled by adding a term for sarcoendoplasmatic reticulum Ca^{2+}-ATPases (SERCAs) activity.

The modified TO model of Ca^{2+} signaling is given in Eqs. A1–A3. We present the unscaled model for clarity. Dimensionless time and space were obtained in the standard manner by scaling with epsilon and the square root of (diffusion coefficient)/epsilon.

$$\frac{\partial c}{\partial t} = \left(P_r^{leak} + P_r^{chan} \frac{c(1-n)}{c + \beta_1(1+\beta_0)} \right)$$

$$\cdot \left((1 + v_m + v_r)C_M - v_m m - (1 + v_r)c \right) - v_r P_r^{max} \frac{c^2}{K_r^2 + c^2}$$

$$- v_m \left(V_{max}^{(1)} \frac{c^2}{K_d^2 + c^2} - V_{max}^{(2)} \frac{[Na^+]^2}{K_{Na}^2 + [Na^+]^2} \frac{m}{K_m + m} \right) + D\nabla^2 c$$

$$(A1)$$

$$\frac{\partial n}{\partial t} = \epsilon \left(\frac{c^2(1-n)}{\beta_2(c + \beta_1(1+\beta_0))} - n \right) \qquad (A2)$$

$$\frac{\partial m}{\partial t} = V_{max}^{(1)} \frac{c^2}{K_d^2 + c^2} - V_{max}^{(2)} \frac{[Na^+]^2}{K_{Na}^2 + [Na^+]^2} \frac{m}{K_m + m} \quad (A3)$$

The Ca^{2+} concentrations in the cytosol, ER, and mitochondria are denoted c, c_r, and m, respectively. The ratio of the effective volume of the ER to the cytosolic is $v_r = 0.185$. The effective volume of all mitochondria to the cytosolic volume is $v_m = 0.1$. C_M is the total amount of Ca^{2+} in the oocyte ($c + v_r c_r + v_m m$) divided by the cell volume ($1 + v_r + v_m$). $C_M = 1.56$ μM and is assumed constant (i.e., no Ca^{2+} flux occurs across the cell membrane). This allows the Ca^{2+} concentration inside the ER to be represented by $c_r = ((1 + v_r + v_m)C_M - c - v_m m)/v_r$. Consequently, c_r does not appear explicitly in the equations. $P_r^{leak} = 0.0097$ s^{-1} is the leakage permeability coefficient of the ER. The fraction of inhibited IP$_3$R ion channels is denoted by n. $P_r^{chan} = 3.89$ s^{-1} denotes the channel permeability coefficient of the IP$_3$R. $\beta_0 = 2.96$, $\beta_1 = 0.12$ μM, and $\beta_2 = 0.1$ μM are the dissociation constants for binding of IP$_3$ to the IP$_3$R, Ca^{2+} to the activating site and Ca^{2+} to the inhibiting site of the IP$_3$R, respectively. β_0 depends on the IP$_3$ concentration (=0.27 μM, see Tang et al. (1996) for details). $\epsilon = 0.15$ s^{-1} is the rate constant for the release of Ca^{2+} from the inhibiting site of the IP$_3$R. For the Ca^{2+}-ATPases in the ER, $P_r^{max} = 5.31$ μM s^{-1} is the maximum pump rate of the SERCAs and $K_r = 0.0296$ μM is the corresponding half-maximum value. $D = 50$ μm^2 s^{-1} is the effective diffusion coefficient of Ca^{2+}. For mitochondrial Ca^{2+} uptake, $V_{max}^{(1)}$ was varied according to the change of mitochondrial uptake in experiments, and the half-maximum value of mitochondrial Ca^{2+} uptake is $K_d = 1.5$ μM. For mitochondrial Ca^{2+} efflux, the maximum release velocity of the Na$^+$/Ca^{2+} exchanger is $V_{max}^{(2)} = 3$ μM s^{-1} and the half-maximum value of its dependence on m is $K_m = 1$ μM. The Na$^+$ concentration is 10 mM and the half-maximum value of the Na$^+$ concentration dependence of the Na$^+$/Ca^{2+} exchanger is $K_{Na} = 5$ mM; ∇ denotes the nabla operator.

REFERENCES

Allbritton, N. L., T. Meyer, and L. Stryer. 1992. Range of messenger action of calcium ion and inositol 1,4,5-trisphosphate. *Science.* 258: 1812–1815.

Amundson, J., and D. Clapham. 1993. Calcium waves. *Curr. Opin. Neurobiol.* 3:375–382.

Atri, A., J. Amundson, D. Clapham, and J. Sneyd. 1993. A single-pool model for intracellular calcium oscillations and waves in the *Xenopus laevis* oocyte. *Biophys. J.* 65:1727–1793.

Berridge, M. J. 1993. Inositol trisphosphate and calcium signaling. *Nature.* 361:315–325.

Bezprozvanny, I., J. Watras, and B. E. Ehrlich. 1991. Bell-shaped calcium-response curves of Ins(1,4,5)P$_3$- and calcium-gated channels from endoplasmic reticulum of cerebellum. *Nature.* 351:751–754.

Blatter, L. A., and W. G. Wier. 1992. Agonist-induced [Ca^{2+}]$_i$ waves and Ca$^{(2+)}$-induced Ca^{2+} release in mammalian vascular smooth muscle cells. *Am. J. Physiol.* 263:H576–H586.

Bygrave, F. L., K. C. Reed, and T. Spencer. 1971. Cooperative interactions in energy-dependent accumulation of Ca^{2+} by isolated rat liver mitochondria. *Nat. New Biol.* 230:89.

Camacho, P., and J. Lechleiter. 1993. Increased frequency of calcium waves in *Xenopus laevis* oocytes that express a calcium-ATPase. *Science.* 260:226–229.

Camacho, P., and J. D. Lechleiter. 1995. Spiral calcium waves: implications for signaling. *In* Calcium Waves, Gradients and Oscillations. Wiley, Chichester. 66–84.

Clapham, D. E. 1995. Ca^{2+} signaling. *Cell.* 80:259–268.

Cornell-Bell, A. H., S. M. Finkbeiner, M. S. Cooper, and S. J. Smith. 1990. Glutamate induces calcium waves in cultured astrocytes: long-range glial signaling. *Science.* 247:470–473.

Davidenko, J. M., A. M. Pertsov, R. Salomonsz, W. Baxter, and J. Jalife. 1992. Stationary and drifting spiral waves of excitation in isolated cardiac muscle. *Nature.* 355:349–351.

DeLisle, S., and M. J. Welsch. 1992. Inositol trisphosphate is required for propagation of calcium waves in *Xenopus* oocytes. *J. Biol. Chem.* 267:7963–7966.

Devreotes, P. N., M. J. Potel, and S. A. Mackay. 1983. Quantitative analysis of cyclic AMP waves mediating aggregation in *Dictyostelium discoideum. Dev. Biol.* 96:405–415.

DeYoung, G. W., and J. Keizer. 1992. A single-pool inositol 1,4,5-trisphosphate-receptor-based model for agonist-stimulated oscillations in Ca^{2+} concentration. *Proc. Natl. Acad. Sci. USA.* 89:9895–9899.

Dockery, J. D., J. P. Keener, and J. J. Tyson. 1988. Dispersion of traveling waves in the Belousov-Zhabotinskii reaction. *Physica D.* 30:177–191.

Dolmetsch, R. E., K. Xu, and R. S. Lewis. 1998. Calcium oscillations increase the efficiency and specificity of gene expression [see comments]. *Nature.* 392:933–936.

Dupont, G., M. J. Berridge, and A. Goldbeter. 1991. Signal-induced Ca^{2+} oscillations: properties of a model based on Ca^{2+}-induced Ca^{2+} release. *Cell Calcium.* 12:73–85.

Eidne, K. A., J. Zabavnik, W. T. Allan, A. J. Trewavas, N. D. Read, and L. Anderson. 1994. Calcium waves and dynamics visualized by confocal microscopy in *Xenopus* oocytes expressing cloned TRH receptors. *J. Neuroendocrinol.* 6:173–178.

Fewtrell, C. 1993. Ca^{2+} oscillations in non-excitable cells. *Annu. Rev. Physiol.* 55:427–454.

Finch, E. A., T. J. Turner, and S. M. Goldin. 1991. Calcium as a coagonist of inositol 1,4,5-trisphosphate-induced calcium release. *Science.* 252:443–446.

Fontanilla, R. A., and R. Nuccitelli. 1998. Characterization of the sperm-induced calcium wave in *Xenopus* eggs using confocal microscopy. *Biophys. J.* 75:2079–2087.

Goroleva, N. A., and J. Bures. 1983. Spiral waves of spreading depression in the isolated chicken retina. *J. Neurobiol.* 14:353–363.

Gu, X., and N. C. Spitzer. 1995. Distinct aspects of neuronal differentiation encoded by frequency of spontaneous Ca^{2+} transients. *Nature.* 375:784–787.

Gunter, T. E., and D. R. Pfeiffer. 1990. Mechanisms by which mitochondria transport calcium. *Am. J. Physiol.* 258:C755–C786.

Harris-White, M. E., S. A. Zanotti, S. A. Frautschy, and A. C. Charles. 1998. Spiral intercellular calcium waves in hippocampal slice cultures. *J. Neurophysiol.* 79:1045–1052.

Hehl, S., A. Golard, and B. Hille. 1996. Involvement of mitochondria in intracellular calcium sequestration by rat gonadotropes. *Cell Calcium.* 20:515–529.

Herrington, J., Y. B. Park, D. F. Babcock, and B. Hille. 1996. Dominant role of mitochondria in clearance of large Ca^{2+} loads from rat adrenal chromaffin cells. *Neuron.* 16:219–228.

Iino, M. 1990. Biphasic Ca^{2+} dependence of inositol 1,4,5-trisphosphate-induced Ca^{2+} release in smooth muscle cells of the guinea pig *taenia caeci. J. Gen. Physiol.* 95:1103–1122.

Jouaville, L. S., F. Ichas, E. L. Holmuhamedov, P. Camacho, and J. D. Lechleiter. 1995. Synchronization of calcium waves by mitochondrial substrates in *Xenopus laevis* oocytes. *Nature.* 377:438–441.

Karma, A. 1994. Electrical alternans and spiral wave breakup in cardiac tissue. *Chaos* 4:461–469.

Kasai, H., and G. J. Augustine. 1990. Cytosolic Ca^{2+} gradients triggering unidirectional fluid secretion from exocrine pancreas. *Nature.* 348:735–738.

Lechleiter, J. D., L. M. John, and P. Camacho. 1998. Ca^{2+} wave dispersion and spiral wave entrainment in *Xenopus laevis* oocytes overexpressing Ca^{2+} ATPases. *Biophys. Chem.* 72:123–129.

Lechleiter, J. D., and D. E. Clapham. 1992. Molecular mechanisms of intracellular calcium excitability in *X. laevis* oocytes. *Cell.* 69:283–294.

Lechleiter, J., S. Girard, D. Clapham, and E. Peralta. 1991. Subcellular patterns of calcium release determined by G protein-specific residues of muscarinic receptors. *Nature.* 350:505–508.

Lechleiter, J., S. Girard, E. Peralta, and D. Clapham. 1991. Spiral calcium wave propagation and annihilation in *Xenopus laevis* oocytes. *Science.* 252:123–126.

Li, W., J. Llopis, M. Whitney, G. Zlokarnik, and R. Y. Tsien. 1998. Cell-permeant caged InsP$_3$ ester shows that Ca^{2+} spike frequency can optimize gene expression [see comments]. *Nature.* 392:936–941.

Li, Y. X., and J. Rinzel. 1994. Equations for InsP$_3$ receptor-mediated [Ca^{2+}] oscillations derived from a detailed kinetic model: a Hodgkin-Huxley-like formalism. *J. Theor. Biol.* 166:461–473.

Loomis, W. F. 1979. Biochemistry of aggregation in *Dictyostelium.* A review. *Dev. Biol.* 70:1–12.

Magnus, G., and J. Keizer. 1997. Minimal model of beta-cell mitochondrial Ca^{2+} handling. *Am. J. Physiol.* 273:C717–C733.

Magnus, G., and J. Keizer. 1998a. Model of beta-cell mitochondrial calcium handling and electrical activity. I. Cytoplasmic variables. *Am. J. Physiol.* 274:C1158–C1173.

Magnus, G., and J. Keizer. 1998b. Model of beta-cell mitochondrial calcium handling and electrical activity. II. Mitochondrial variables. *Am. J. Physiol.* 274:C1174–C1184.

Marinos, E. 1985. The number of mitochondria in *Xenopus laevis* ovulated oocytes. *Cell Diff.* 16:139–143.

Marinos, E., and F. S. Billett. 1981. Mitochondrial number, cytochrome oxidase and succinic dehydrogenase activity in *Xenopus laevis* oocytes. *J. Embryol. Exp. Morphol.* 62:395–409.

Mikhailov, A. S. 1994. Foundations of Synergetics I. Springer, Berlin.

Nathanson, M. H., A. D. Burgstahler, A. Mennone, M. B. Fallon, C. B. Gonzalez, and J. C. Saez. 1995. Ca^{2+} waves are organized among hepatocytes in the intact organ. *Am. J. Physiol.* 269:G167–G171.

Newman, E. A., and K. R. Zahs. 1997. Calcium waves in retinal glial cells. *Science.* 275:844–848.

Parker, I., and I. Ivorra. 1990. Inhibition by Ca^{2+} of inositol trisphosphate-mediated Ca^{2+} liberation: a possible mechanism for oscillatory release of Ca^{2+}. *Proc. Natl. Acad. Sci. USA.* 87:260–264.

Pozzan, T., R. Rizzuto, P. Volpe, and J. Meldolesi. 1994. Molecular and cellular physiology of intracellular calcium stores. *Physiol. Rev.* 74:595–636.

Putney, J. W. J., and J. Bird. 1993. The inositol phosphate-calcium signaling system in nonexcitable cells. *Endocrine Rev.* 14:610–631.

Rensing, L. 1993. Oscillations and morphogenesis. *In* Cellular Clock Series. Vol. 5. L. N. Edmunds, Jr., series ed. Marcel Dekker, Inc., New York.

Rizzuto, R., M. Brini, M. Murgia, and T. Pozzan. 1993. Microdomains with high Ca^{2+} close to InsP$_3$-sensitive channels that are sensed by neighboring mitochondria. *Science.* 262:744–747.

Rizzuto, R., A. V. M. Simpson, M. Brini, and T. Pozzan. 1992. Rapid changes of mitochondrial Ca^{2+} revealed by specifically targeted recombinant aequorin. *Nature.* 358:325–327.

Robb-Gaspers, L. D., and A. P. Thomas. 1995. Coordination of Ca^{2+} signaling by intercellular propagation of Ca^{2+} waves in the intact liver. *J. Biol. Chem.* 270:8102–8107.

Sanderson, M. J., A. C. Charles, S. Boitano, and E. R. Dirksen. 1994. Mechanisms and function of intercellular calcium signaling. *Mol. Cell. Endocrinol.* 98:173–187.

Satoh, T., C. A. Ross, A. Villa, S. Supattapone, T. Pozzan, S. H. Snyder, and J. Meldolesi. 1990. The inositol 1,4,5-trisphosphate receptor in cerebellar Purkinje cells: quantitative immunogold labeling reveals concentration in an ER subcompartment. *J. Cell Biol.* 111:615–624.

Scarpa, A., and P. Graziotti. 1973. Mechanisms for intracellular calcium regulation in heart. I. Stopped-flow measurements of Ca^{++} uptake by cardiac mitochondria. *J. Gen. Physiol.* 62:756–772.

Tang, Y., and H. G. Othmer. 1994. A model of calcium dynamics in cardiac myocytes based on the kinetics of ryanodine-sensitive calcium channels. *Biophys. J.* 67:2223–2235.

Tang, Y., and J. Stephenson. 1996. Calcium dynamics and homeostasis in a mathematical model of the principal cell of the cortical collecting tubule. *J. Gen. Physiol.* 107:207–230.

Tang, Y., J. Stephenson, and H. Othmer. 1996. Simplification and analysis of models of calcium dynamics based on IP_3-sensitive calcium channel kinetics. *Biophys. J.* 70:246–263.

Thomas, A. P., G. S. Bird, G. Hajnoczky, L. D. Robb-Gaspers, and J. W. Putney, Jr. 1996. Spatial and temporal aspects of cellular calcium signaling. *FASEB J.* 10:1505–1517.

Thomas, A. P., L. D. Robb-Gaspers, T. A. Rooney, G. Hajnoczky, D. C. Renard-Rooney, and C. Lin. 1995. Spatial organization of oscillating calcium signals in liver. *Biochem. Soc. Trans.* 23:642–648.

Tsien, R. W., and R. Y. Tsien. 1990. Calcium channels, stores, and oscillations. *Annu. Rev. Cell Biol.* 6:715–760.

Wagner, J., Y. X. Li, J. Pearson, and J. Keizer. 1998. Simulation of the fertilization Ca^{2+} wave in *Xenopus laevis* eggs. *Biophys. J.* 75:2088–2097.

Wang, S., and G. Augustine. 1995. Confocal imaging and local photolysis of caged compounds: dual probes of synaptic function. *Neuron.* 15:755–760.

Winfree, A. T. 1993. The Geometry of Excitability. Addison-Wesley, Reading, MA.

Yao, Y., and I. Parker. 1994. Ca^{2+} influx modulation of temporal and spatial patterns of inositol trisphosphate-mediated Ca^{2+} liberation in *Xenopus* oocytes. *J. Physiol. (Lond).* 476:17–28.